Spontaneous cracking of amorphous solid water films and the dependence on microporous structure

Caixia Bu, Catherine A. Dukes, and Raúl A. Baragiola

Citation: Appl. Phys. Lett. **109**, 201902 (2016); doi: 10.1063/1.4967789
View online: http://dx.doi.org/10.1063/1.4967789
View Table of Contents: http://aip.scitation.org/toc/apl/109/20
Published by the American Institute of Physics

Spontaneous cracking of amorphous solid water films and the dependence on microporous structure

Caixia Bu,[a] Catherine A. Dukes, and Raúl A. Baragiola[b]
Laboratory for Astrophysics and Surface Physics, Materials Science and Engineering, University of Virginia, Charlottesville, Virginia 22904, USA

(Received 11 September 2016; accepted 23 October 2016; published online 14 November 2016)

Vapor-deposited, porous, amorphous, water-ice films, also called amorphous solid water (ASW), crack spontaneously during growth when the film thickness exceeds a critical value (L_c). We measured the L_c during growth of ASW films as a function of growth temperature ($T_g = 10$ K, 30 K, and 50 K) and deposition angle ($\theta = 0°$, 45°, and 55°) using a quartz crystal microbalance, an optical interferometer, and an infrared spectrometer. The critical thickness, 1–5 μm under our experimental conditions, increases with T_g and θ, an indication of film porosity. We suggest that ASW films undergo tensile stress due to the mismatch between substrate adhesion and contracting forces derived from the incompletely coordinated molecules on the surfaces of the pores. We provide a model to explain the observed dependences of L_c on the T_g and θ in the context of Griffith theory and estimate the tensile strength of low-temperature ASW to be ~25–40 MPa. Our model can be applied more generally to describe fracture of other solids with microporous structures, such as metallic or ceramic materials with voids. *Published by AIP Publishing.*
[http://dx.doi.org/10.1063/1.4967789]

Amorphous solid water (ASW), observed in comets, planets, and satellites of the outer solar system, and on dust grains in the cold interstellar medium,[1,2] is formed in the laboratory by condensation of water vapor onto substrates colder than ~130 K under ultra-high vacuum (UHV). A crucial characteristic of ASW is its microporous structure,[3] attributed to molecular shadowing and limited diffusion at low temperatures as shown by cluster calculations[4] and ballistic simulations.[5,6] The pore structure of ASW has been studied experimentally by measuring gas uptake,[3,7–9] density,[10,11] infrared (IR) absorption of dangling OH bonds (DBs),[8,9,11–13] positron annihilation,[14] and neutron scattering.[15] It is known that the porosity of ASW depends strongly on the growth temperature (T_g),[3,7,11] deposition angle (θ),[5–9,11,13] incident atom collision energy,[16] and subsequent processing such as annealing[11,13–15] or ion irradiation.[17] However, direct experimental measurements of the pore morphology such as physical shape (radii, length, interconnectivity, etc.) and size distribution remain incomplete, particularly at <77 K.

The elastic properties of ASW films deposited at 80–130 K are affected by their porosity.[18] As T_g increases, the shear modulus grows and internal friction decreases, suggesting enhanced mechanical stability and reduced local atomic disorder with reduced porosity, respectively.[18] However, the dependences of fracture strength on porosity of ASW have not been explored and could have implications for other porous films at temperatures >100 K. For instance, microstructures in vapor-deposited metal films[19] can result in intrinsic stresses leading to mechanical failure,[20] impeding their application as coatings, transistors, microcircuits, and so on. Similarly, void-induced cracks in ceramic materials[21] can lead to potentially dangerous failures in thermal or electrical insulators.

Laboratory-prepared thin ($\leq$1.5 μm) ASW films are transparent with negligible scattering in the visible-infrared ranges, as inferred pore dimensions (~2 nm)[13,15] are much smaller than the wavelength. However, cracks—wide boundaries between particles at scales comparable to or larger than the wavelength—can strongly affect optical reflectance and result in a frosty appearance. Thus, ASW fracture is of particular importance in remote sensing, as compositional information for extraterrestrial objects is primarily derived from reflected sunlight. For mixtures of ASW and volatiles, crystallization-induced cracking has been reported at ~150 K during temperature programmed desorption.[22–24] The formation of cracks has been reported in earlier laboratory studies during growth of ASW films, with thickness from ~1–2 μm at 20 K to ~10–30 μm above 80 K; however, reported critical thicknesses and temperatures are not consistent and the underlying mechanism initiating the fracture remains unclear.[25–27]

Here, we investigate ASW film fracture during growth, using vacuum quartz crystal microbalance (QCM),[28] interferometry, optical microscopy, and IR spectroscopy. Based on our results, we extend Griffith theory to correlate microporous structure with cracking extent and mechanical strength.

Experiments were conducted in an UHV system[29,30] with a pressure of $\sim 2 \times 10^{-10}$ Torr. ASW films were deposited by directing degassed HPLC (High Performance Liquid Chromatography)-grade water (H_2O) vapor through a microcapillary array doser[31] onto a liquid-helium-cooled QCM (the substrate) mounted on a copper block. The QCM is coated with a 100-nm-thick, optically flat layer of gold, and the doser is designed such that molecules condense uniformly over the QCM sensitive area. The substrate

[a]Author to whom correspondence should be addressed. Electronic mail: cb8nw@virginia.edu
[b]Deceased.

temperature was measured using a silicon-diode temperature sensor inserted in the copper block and regulated with a temperature controller coupled to resistive heaters. The target assembly can be rotated to vary the H_2O-vapor deposition angle (θ, angle between the vapor beam and the substrate normal). With deposition, the QCM resonant frequency (f) changes proportionally to the deposited areal mass, which is subsequently converted into column density (in units of monolayers, $1\,\text{ML} = 1 \times 10^{15}$ molecules/cm^2) with errors of ± 0.08 ML. We use a UV-visible interferometer[17] to determine the film thickness (L) by fitting the reflectance spectra with Fresnel equations,[10] which, together with the areal mass, gives the average film density (ρ, in units of g/cm^3, with errors of ± 0.02). The volumetric porosity, defined as $\phi = 1 - \rho/\rho_c$, is calculated using $\rho_c = 0.94$ g/cm^3 for the density of the intrinsic compact ASW.[32] Any changes of the film morphology were observed *in vacuo*, with a field-of-view equal to 1.4-mm in diameter and a spatial resolution of $\sim 3\,\mu$m, using a long-distance microscope mounted outside the vacuum chamber and a digital camera.[30]

During film growth, the substrate was maintained at a constant growth temperature (T_g); the H_2O-vapor was directed toward the QCM at a fixed θ, and the flux was controlled such that the f decreased at a constant rate of 1.4 ± 0.2 Hz, equal to 0.6 ± 0.1 ML/s. We continuously monitored the QCM f and micron-scale film morphology; film growth was terminated when the f and microscopy images indicated that abrupt morphologic change, cracking, had occurred. The column density at the onset of cracking is termed the "critical column density," while the corresponding thickness is termed the "critical thickness (L_c)." Fig. 1(a) shows the temporal evolution of f during the growth of an ASW film at $T_g = 30$ K and $\theta = 0°$. The bare QCM had an intrinsic resonant frequency f_i, and deposition started at $t = 0$. The L was measured at three frequencies within the region where f decreased *smoothly*, and the derived densities (average $\bar{\rho} = 0.83 \pm 0.02$ g/cm^3) were thickness-independent within experimental errors. The microscope image (Fig. 1(b), left) indicates that the film was transparent without micron-scale structural defects. However, above $\sim$7000 s the f increased *abruptly*, accompanied by the appearance of micron-scale cracks in the ASW films (Fig. 1(b), right). We terminated the deposition after observing these abrupt changes. The QCM measurement after cracking is invalid, as the film is no longer homogeneous and the adhesion is nonuniform.[28] The QCM frequency at the onset of the cracking was f_c, and the critical column density was determined using the frequency change of $\Delta f = |f_i - f_c|$. The spontaneous cracking impeded the direct measurement of the L_c due to loss of the interference patterns. Rather, the L_c was extrapolated using the measured Δf and $\bar{\rho}$. The H_2O flux was halted for $\sim$300 s during thickness measurements, causing minor frequency fluctuations. The time lag has been corrected in Fig. 1(a). We confirmed that the thickness measurements did not affect the resulting L_c.

We deposited ASW films at various T_g and θ and measured the corresponding L_c. With varied θ, densities of the ASW films are significantly different;[5–9,11,13] thus, we use volumetric porosity ϕ as a measure of the microporous structure. However, ASW films deposited at $\theta = 0°$ at different

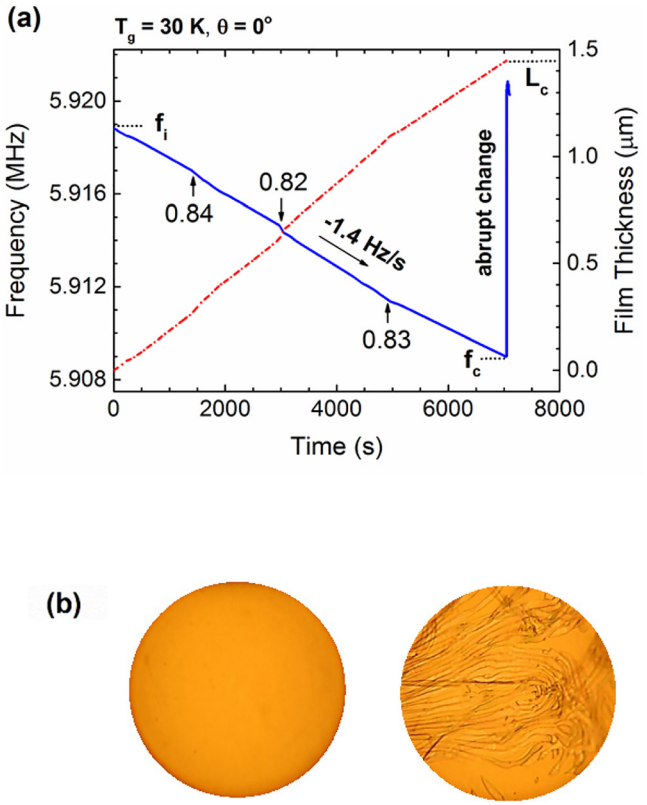

FIG. 1. (a) Temporal evolution of the QCM frequency (f, solid-blue line, left-axis) and the derived film thickness (L, dashed-red line, right-axis) during growth of an ASW film at $T_g = 30$ K at $\theta = 0°$ using a constant water vapor flux. The f, f_i for the bare QCM, decreased at a rate of 1.4 ± 0.2 Hz/s and increased abruptly at f_c; the deposition was terminated after reaching f_c, corresponding to a critical thickness of L_c. Values (± 0.02 g/cm^3) along the frequency curve describe film densities. (b) microscope images of the ASW film below (left) and above (right) L_c.

T_g within 10–50 K have similar ϕ.[7,10] In this case, the microporous structure is characterized by the IR adsorptions of the DBs.[8,9,12,13] We collected IR spectra of 1100-ML-thick ASW films deposited onto a CsI substrate at $\theta = 0°$ for different T_g in a second UHV system.[29,33] Spectra were taken with 2 cm^{-1} resolution in the transmission mode using a Nicolet 670 Fourier transform infrared spectrometer and expressed in optical depth, $-\ln(T/T_o)$, where T is the transmission of the film-CsI system, and T_o is that through the bare CsI substrate. The substrate material does not affect the IR features of DBs of the ice films. The selected film thickness is sufficient to obtain high quality IR spectra but thin enough to avoid the potential spontaneous cracking.

The porosity, an indicator of the volume fraction of the pores in the ASW films, increases with the θ.[7,11,13] Thus, we deposited ASW films at $T_g = 30$ K at different θ of 0°, 45°, and 55°. The dependences of critical thickness (L_c) and porosity (ϕ) on θ (Fig. 2) suggest that the L_c may be directly related to ϕ. The same correlation between L_c and θ was also observed in our laboratory for ice films deposited at $T_g = 20$ K with θ between 0° and 70°.[34]

The T_g also affects the ASW microporous structure,[3,7] as the increased surface diffusion at higher T_g can impede the pore formation.[4,6] We investigate the effects of T_g on the spontaneous cracking by depositing ASW films at different T_g (10, 30, and 50 K) at $\theta = 0°$. The L_c as a function of T_g is

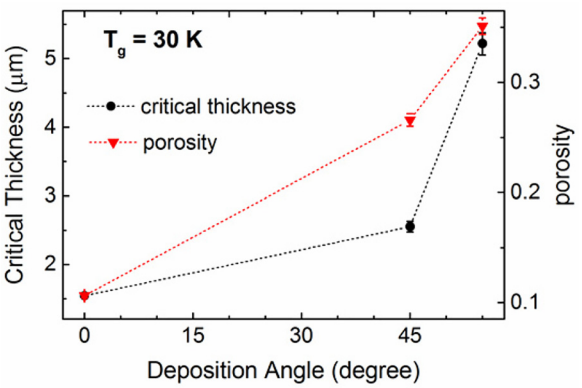

FIG. 2. Dependence of the critical thickness (left-axis) and porosity (right-axis) on the deposition angle at 30 K.

shown in Fig. 3(a). Unlike the case in Fig. 2, the measured volumetric densities of these films were identical ($0.83 \pm 0.02\,\mathrm{g/cm^3}$) within experimental error, consistent with earlier studies.[7,10] Thus, for enhanced sensitivity, we adopted IR absorptions of the DBs to characterize the extent of the microporous structure. DB1 at $\sim 3720\,\mathrm{cm^{-1}}$ and DB2 at $\sim 3692\,\mathrm{cm^{-1}}$ are assigned to the two- and three-coordinated water molecules, respectively, lining the pore surfaces,[4,12] and here we consider the integrated area of these DBs as a measure of the total internal surface area (ISA) of the ASW films, a method used previously by several groups.[8,9,11–13] Fig. 3(b) shows the IR spectra of 1100-ML-thick ASW films, and the derived DBs areas are presented in Fig. 3(a). A similar trend was measured for ASW for $\theta = 45°$. These results suggest that the L_c increases with decreased ISA and appear contrary to the data in Fig. 2, since ISA is expected to increase with θ.[7–9,11,13]

Microstructure and residual stresses are of critical importance to the elastic properties of a material, which affect the technological application. In plasma-sprayed ceramic-coatings, nano- and micron-sized defects are formed by thermal contraction stresses, degrading the fracture strength to ~45%.[35] For metal and semiconductor films deposited in the Volmer-Weber mode, a zipping model is used to describe the origin of the tensile stresses generated when discrete islands coalesce and

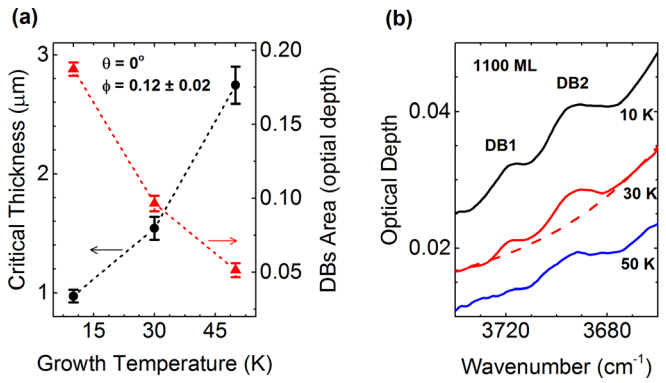

FIG. 3. (a) Growth-temperature (T_g) dependences of the critical thickness (L_c, circles) and the area of the dangling bond features (DBs area, triangles). ASW films were deposited at $\theta = 0°$, with identical volumetric porosities of $\phi = 0.12 \pm 0.02$. (b) IR spectra of 1100-ML ASW films at different T_g. The spectrum for $T_g = 50$ K has been shifted down (by −0.01) for clarity. DB1 and DB2 areas, DBs area in (a)-panel, are calculated after subtraction of the appropriate polynomial baselines (dashed line).

deform upon contact to reduce surface energy at the expense of stored elastic energy.[36–38] Tensile stresses can be dissipated by film fracture or over-layer pealing from the substrate. For brittle crystalline materials, the tensile stresses result in fractures along the cleavage plane, but amorphous structures undergo conchoidal fracture in the direction normal to the stress.[39]

The mechanical strength of a material depends on various parameters, including the elastic modulus, surface energy, and film morphology. The presence of very small, microscopic flaws (voids or pores) lowers the mechanical strength, as demonstrated in Griffith's studies using glass specimens with artificial, linear, surface flaws.[40] Stress tests by Griffith showed that for brittle materials, at fracture, the product of the square root of the crack length (a) and the stress perpendicular to the crack (σ_f) was nearly constant (C), $\sigma_f \sqrt{a} \approx \mathrm{C}$, with no dependence on stresses parallel to crack. Griffith explained this relationship by considering the changes in the system energy associated with incremental crack extension. Briefly, when a solid under stress cracks, the total elastic energy is reduced, while the total surface energy increases as a result of molecular bond breaking to form new surfaces (two per crack). Griffith's criterion was that catastrophic fractures occur when the magnitude of the elastic energy is greater than the total surface energy. This criterion led to the Griffith equation describing the empirical relationship between the applied stress (σ) and a critical flaw length (a_c), i.e., when it becomes energetically favorable for tiny inherent cracks or defects to propagate

$$a_c = \frac{2\gamma E}{\pi \sigma^2}, \tag{1}$$

where γ is the surface energy and E is Young's modulus. Thus, if the initial flaw (a) increases in length while remaining less than a_c, the material remains intact; however, where $a \geq a_c$, the growth of crack is spontaneous and catastrophic. While Griffith's original work dealt solely with highly brittle materials such as glass, this model was later modified independently by Irwin[41] and Orowan[42] for applications in more ductile materials.

Water molecules in bulk ice are held together by tetrahedral hydrogen bonding.[43] In the vicinity of the surface, this tetrahedral-hydrogen structure is broken, resulting in incompletely coordinated molecules with dangling O or H atoms. The incompletely coordinated molecules, insignificant in crystalline ice, are abundant in ASW due to the large pore surface areas,[3,7–9,13] manifesting as enhanced IR features of the DBs.[4,12] Molecules in porous ASW have a greater average separation and higher system energy relative to those in the compact state, deriving from the presence of pores and short-range attractive interaction between the incompletely coordinated molecules on the pore walls.[4,12,44] To minimize the system energy, ASW films tend to contract. However, this tendency is constrained by adhesion of the films to the rigid substrate which, in turn, applies a tensile stress on the films. The magnitude of the attractive force—due primarily to intermolecular hydrogen bonding—outweighs any repulsive electrostatic forces such as dipole-dipole interactions of aligned H_2O on pore surfaces, since these interactions decay

significantly with intermolecular distance (r), proportional to $\sim 1/r^3$ compared to $\sim 1/r^2$ for hydrogen bonding,[45] and $<10\%$ of surface molecules contribute to the aligned dipoles.[29,46] Thus, we suggest that overall tensile stresses develop in ASW films due to the presence of nanopores.

In the context of Griffith theory, we examine our observations that the L_c, an upper limit proxy for a_c, increases with θ and T_g (Figs. 2 and 3). In our model, the pores, accessible from the vacuum-film interface as indicated by the gas absorption experiments,[3,7–9,13] lengthen linearly with the increased film thickness during growth. Since the tensile stress (σ) originates from the interactions of incompletely coordinated molecules, based on Eq. (1) we expect the L_c to decrease with increased abundance of these molecules. This is consistent with observations in Fig. 3(a) that L_c increases with T_g, since Fig. 3(b) clearly shows that two- and three-coordinated molecules reduce with increased T_g. As the θ increases, IR measurements show enhancement of the DB intensities,[11,13] and we expect reduced L_c, in contrast to Fig. 2. However, this picture is over-simplified, since it does not take into account the pore geometry or size distribution. Pores are expected to be inclined in the deposition direction (Fig. 4), with an angle β slightly smaller than θ and increasing with θ,[5,6,19] and it is only the radial stress [$\sigma' = \cos(\beta) \times \sigma$, normal to the pores] that contributes to the sample fracture.[40] In this scenario, the effective stress σ' reduces with increasing θ. Thus, we conclude that the increase of L_c with θ in Fig. 2 is not inconsistent with the Griffith model but results from the competition between the abundance of incompletely coordinated molecules and the inclination of the pores. Therefore, Eq. (1) can be used qualitatively to explain all observations in Figs. 2 and 3.

The physical parameters γ, E, and σ are unknown for ASW at ≤ 50 K although Young's modulus for compact polycrystalline ice (at 257 K) has been measured: $E_o \approx 9$ GPa.[43] For ASW with porosity ϕ, as suggested by Hessinger *et al.*,[18] E can be estimated empirically with following equation:[39]

$$E = E_o(1 - 1.9\phi + 0.9\phi^2). \quad (2)$$

We estimate the magnitude of the σ on porous ASW deposited at $T_g = 30$ K for $\theta = 0°$, using Eqs. (1) and (2) in combination with our measured critical thickness ($a_c = L_c$).

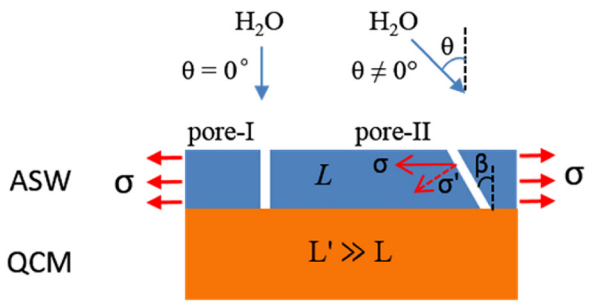

FIG. 4. Tensile stress (σ) applied in ASW films during growth on the QCM (thickness $L' \gg L$), due to the pores. Based on ballistic simulations,[5,6] the majority of the pores are normal to the substrate (pore-I) with deposition angle $\theta = 0°$; as the θ deviates from normal ($\theta \neq 0°$), the pores tilt toward the direction of deposition (pore-II), with an angle β somewhat smaller than θ. The effective stress contributing to cracking changes from σ in pore-I to $\sigma' = \cos(\beta) \times \sigma$ in pore-II.

In this case, L_c is 1.54 μm and ϕ is 0.12, implying that E is 7 GPa from Eq. (2). Without details of the pore morphology, the surface energy γ can be only approximated with a simplified model—molecules on the pore surfaces are two-coordinated (three-coordinated molecules are also expected but less abundant)[4] and γ is the energy density of the broken hydrogen bonds (two per surface molecule). The energy per hydrogen bond is 0.24 eV;[43] thus, the γ due to the two-coordinated molecules is approximately 0.51 J/m^2, assuming that each water molecule occupies an area of $S_o = \pi (d/2)^2 \approx 1.5 \times 10^{-19}$ m^2 (where d is the molecule diameter, ~ 4.4 Å).[47] The tensile strength σ of the porous ASW ($\phi = 0.12$) can thus be estimated with Eq. (1) as $\sigma = 38$ MPa, using the measured L_c, in conjunction with calculated E and γ. This value is rather smaller than other amorphous solids, such as glass which has a tensile strength of $\sigma \approx 70$ MPa and porous ceramic ($\phi \approx 0.1$) of $\sigma \approx 150$ MPa at room temperature,[39] underlining the fragile nature of ASW. The estimated tensile strength for ASW is at least one order of magnitude larger than the fracture toughness of polycrystalline ice, $\sim$0.5–1.5 MPa measured at 263 K.[43] This variation in ice mechanical strength with phase is expected, since amorphous metals and alloys typically show significant enhancements in tensile strength relative to their crystalline phases.[48] We note the structural failure of ASW atop volatiles, which occurs at $\sim$0.25 MPa at $\gtrsim$100 K,[23] is due to the pressure from sublimation of the underlying layer, a different mechanism than the tensile stresses discussed here.

For ASW films deposited at $T_g = 30$ K at $\theta = 45°$, L_c is 2.24 μm and ϕ is 0.27; our model provides an effective tensile strength $\sigma' = 27$ MPa. This value is less than for $\theta = 0°$ ($\phi = 0.12$), as E decreases and the L_c increases with higher porosity. This trend is consistent with observations in other materials that fracture strength decreases with volumetric porosity.[39]

In summary, vapor-deposited amorphous solid water (ASW) films crack spontaneously during growth when the thickness exceeds a critical value (L_c). The formation of cracks in ASW, reported in earlier studies at $\gtrsim$150 K, was attributed to ice phase transformation.[22,23,49,50] Our observations indicate that the formation of cracks in micron-thick ASW can occur at temperatures well below the phase transformation temperature. For ASW films deposited at deposition angle $\theta = 0°$, the L_c increases from $\sim$1.0 to 2.8 μm as the growth temperature (T_g) increases from 10 to 50 K; at $T_g = 30$ K, the L_c increases from $\sim$1.5 to 5.3 μm as the θ increases from 0° to 55°. We suggest that porous ASW films are under tensile stresses, originating from the imbalance between film adhesion to the substrate and the attractive forces between the incompletely coordinated molecules on the pore surfaces. The stress initiates spontaneous, catastrophic fracture, a fundamental consequence of the ASW porous structure. We propose a mechanism, based on the micro-porous nature of ASW films, to qualitatively explain our observations in the context of Griffith theory. These concepts are expected to be generally applicable to other non-ductile solids, such as ceramics and glasses, with microporous structures.

This work was supported by NASA's Outer Planets Research and LASER Programs. The authors thank Dr. U. Raut and Dr. E. Mitchell for useful discussions and

assistance with dangling bond measurements. The authors acknowledge the helpful comments of the anonymous reviewers. During the preparation of the manuscript, co-author Raúl A. Baragiola unexpectedly passed away. Without Raúl's encouragement and oversight, this work would not have been completed—his thoughts and contributions were invaluable, as well as our many office and home discussions.

[1]T. L. Roush, J. Geophys. Res. **106**(E12), 33315, doi:10.1029/2000JE001334 (2001).
[2]R. A. Baragiola, Planet. Space Sci. **51**, 953 (2003).
[3]E. Mayer and R. Pletzer, Nature **319**, 298 (1986).
[4]V. Buch, J. Chem. Phys. **96**(5), 3814 (1992).
[5]G. A. Kimmel, Z. Dohnalek, K. P. Stevenson, R. S. Smith, and B. D. Kay, J. Chem. Phys. **114**, 5295 (2001).
[6]Z. Dohnalek, G. A. Kimmel, P. Ayotte, R. S. Smith, and B. D. Kay, J. Chem. Phys. **118**, 364 (2003).
[7]K. P. Stevenson, G. A. Kimmel, Z. Dohnalek, R. S. Smith, and B. D. Kay, Science **283**, 1505 (1999).
[8]T. Zubkov, R. S. Smith, T. R. Engstrom, and B. D. Kay, J. Chem. Phys. **127**, 184707 (2007).
[9]T. Zubkov, R. S. Smith, T. R. Engstrom, and B. D. Kay, J. Chem. Phys. **127**, 184708 (2007).
[10]M. S. Westley, G. A. Baratta, and R. A. Baragiola, J. Chem. Phys. **108**, 3321 (1998).
[11]J. B. Boss, K. Isokoski, M. S. de Valois, and H. Linnartz, Astron. Astrophys. **545**, A82 (2012).
[12]V. Buch and J. P. Devlin, J. Chem. Phys. **94**, 4091 (1991).
[13]U. Raut, M. Fama, B. D. Teolis, and R. A. Baragiola, J. Chem. Phys. **127**, 204713 (2007).
[14]Y. C. Wu, J. Jiang, S. J. Wang, A. Kallis, and P. G. Coleman, Phys. Rev. B **84**, 064123 (2011).
[15]C. R. Hill, C. Mitterdorfer, T. G. A. Youngs, D. T. Bowron, H. J. Franser, and T. Loerting, Phys. Rev. Lett. **116**, 215501 (2016).
[16]R. S. Smith, T. Zubkov, Z. Dohnalek, and B. D. Kay, J. Chem. Phys. B **113**, 4000 (2009).
[17]U. Raut, M. Fama, M. J. Loeffler, and R. A. Baragiola, Astrophys. J. **687**, 1070 (2008).
[18]J. Hessinger, B. E. White, Jr., and R. O. Pohl, Planet. Space Sci. **44**(9), 937 (1996).
[19]A. G. Dirks and H. J. Leamy, Thin Solid Films **47**, 219 (1977).
[20]R. W. Hoffman, Thin Solid Films **34**, 185 (1976).
[21]R. W. Rice, J. Mater. Sci. **31**, 1969–1983 (1996).
[22]R. S. Smith, C. Huang, E. K. L. Wong, and B. D. Kay, Phys. Rev. Lett. **79**, 909 (1997).
[23]R. A. May, R. S. Smith, and B. D. Kay, J. Chem. Phys. **138**, 104502 (2013).
[24]C. Bu and R. A. Baragiola, in *46th Lunar and Planetary Science Conference* (2015), p. 2956.
[25]B. E. Wood and J. A. Roux, J. Opt. Soc. Am. **72**, 720 (1982).
[26]D. Laufer, E. Kochavi, and A. Bar-Nun, Phys. Rev. B **36**, 9219 (1987).
[27]B. Schmitt, J. Ocampo, and J. Klinger, J. Phys. Colloques **48**(C1), 519 (1987).
[28]M. A. Allodi, R. A. Baragiola, G. A. Baratta, M. A. Barucci, G. A. Blake, P. Buduch, J. R. Brucato, C. Contreras, S. H. Cuylle, D. Fulvio *et al.*, Space Sci. Rev. **180**, 101 (2013).
[29]C. Bu, J. Shi, U. Raut, E. H. Mitchell, and R. A. Baragiola, J. Chem. Phys. **142**, 134702 (2015).
[30]C. Bu, D. A. Bahr, C. A. Dukes, and R. A. Baragiola, Astrophys. J. **825**, 106 (2016).
[31]N. J. Sack and R. A. Baragiola, Phys. Rev. B **48**, 9973 (1993).
[32]A. H. Narten, C. G. Venkatesh, and S. A. Rice, J. Chem. Phys. **64**, 1106 (1976).
[33]U. Raut, E. H. Mitchell, and R. A. Baragiola, Astrophys. J. **811**, 120 (2015).
[34]D. Pugh, M.S. thesis, University of Virginia, 2002.
[35]R. McPherson, Surf. Coat. Technol. **39/40**, 173 (1989).
[36]W. B. Nix and B. M. Clemens, J. Mater. Res. **14**, 3467 (1999).
[37]L. B. Freund and E. Chason, J. Appl. Phys. **89**, 4866 (2001).
[38]J. A. Floro, P. G. Kotula, and S. C. Seel, Phys. Rev. Lett. **91**, 096101 (2003).
[39]W. D. Callister, Jr., *Materials Science and Engineering: An Introduction*, 7th ed. (John Wiley & Sons, 2007).
[40]A. A. Griffith, Philos. Trans. R. Soc. London **221**, 163 (1921).
[41]G. R. Irwin, J. Appl. Mech. **24**, 361–364 (1957).
[42]E. Orowan, Rep. Prog. Phys. **12**, 185 (1949).
[43]V. F. Petrenko and R. W. Whitworth, *Physics of Ice* (Oxford University Press, 1999).
[44]B. W. Sheldon, A. Lau, and A. Rajamani, J. Appl. Phys. **90**, 5097 (2001).
[45]J. N. Israelachvili, *Intermolecular and Surface Forces* (Academic Press, London, 2011).
[46]M. J. Iedema, M. J. Dresser, D. L. Doering, J. B. Rowland, W. P. Hess, A. A. Tesekouras, and J. P. Cowin, J. Phys. Chem. B **102**, 9203 (1998).
[47]D. Pan, L.-M. Liu, G. A. Tribello, B. Slater, A. Michaelides, and E. Wang, Phys. Rev. Lett. **101**, 155703 (2008).
[48]W. L. Johnson, J. Miner., Met. Mater. Soc. **54**(3), 40–43 (2002).
[49]J. A. Ghormley and C. J. Hochanadel, Science **171**, 62 (1971).
[50]T. C. Sivakumar, S. A. Rice, and M. G. Sceats, J. Chem. Phys. **69**, 3468 (1978).